A $La_{2-x}Gd_xZr_2O_7$ layer deposited by chemical solution : a promising seed layer for the fabrication of high Jc and low cost coated conductors

Reference:

Muguerra Hervé, Pescheux Anne-Claire, Meledin Alexander, van Tendeloo Gustaaf, Soubeyroux Jean-Louis.- A $La_{2-x}Gd_xZr_2O_7$ layer deposited by chemical solution : a promising seed layer for the fabrication of high Jc and low cost coated conductors

Journal of materials chemistry C : materials for optical and electronic devices - ISSN 2050-7534 - 3:44(2015), p. 11766-11772

Full text (Publishers DOI): http://dx.doi.org/doi:10.1039/C5TC03365A

Journal of Materials Chemistry C

La2-xGdxZr2O7 layer deposited by chemical solution: A promising seed layer for the fabrication of high Jc and low cost coated conductors.

Journal:	*Journal of Materials Chemistry C*
Manuscript ID	TC-ART-10-2015-003365
Article Type:	Paper
Date Submitted by the Author:	16-Oct-2015

Complete List of Authors:	Muguerra, Hervé; Institut Néel, Pescheux, Anne-Claire; Institut Néel Meledin, Alexander; University of Antwerp, Electron Microscopy for Material Science (EMAT) Van Tendeloo, Gustaaf; University of Antwerp, (Electron Microscopy for Materials Science Soubeyroux, Jean-louis; Institut Néel,

Journal of Materials Chemistry C

ARTICLE

$La_{2-x}Gd_xZr_2O_7$ layer deposited by chemical solution: A promising seed layer for the fabrication of high Jc and low cost coated conductors.

Received 00th January 20xx,
Accepted 00th January 20xx

DOI: 10.1039/x0xx00000x

www.rsc.org/

Hervé Muguerra,[*ab] Anne-Claire Pescheux,[ab] Alexander Meledin,[c] Gustaaf Van Tendeloo,[c] and Jean-Louis Soubeyroux[ab]

We deposited $La_{2-x}Gd_xZr_2O_7$ seed layers by chemical solution method on a Ni-5%W substrate to study the influence of these layers on the growth process of a 60-nm-thick $La_2Zr_2O_7$ layer. We measured the performances of these new buffer layers integrated in a coated conductor with a 300-nm-thick $Y_{0.5}Gd_{0.5}Ba_2Cu_3O_{7-x}$ layer. For the seed layers, we considered two different gadolinium contents (x = 0.2 and x = 0.8) and three different thickness for these compositions (20 nm, 40 nm, 60 nm). The most promising buffer layer stacks are those with 20 nm of $La_{1.8}Gd_{0.2}Zr_2O_7$ layer or $La_{1.2}Gd_{0.8}Zr_2O_7$. Indeed the $La_{2-x}Gd_xZr_2O_7/La_2Zr_2O_7$ films are highly textured, similar to a 100-nm-thick $La_2Zr_2O_7$ layer, but their roughness is four times lower. Moreover it contains less and smaller pores in the seed layer than a pure $La_2Zr_2O_7$ layer. The surface of the $La_2Zr_2O_7$ is also homogenous and crystalline with an orientation deviation from the ideal <011> (100) direction below 10°. With the 20 nm $La_{2-x}Gd_xZr_2O_7$ seed layers we obtain in the coated conductors an efficient textured transfer with no gradual degradation from the substrate throughout the superconducting layer. The highest Tc and Jc values are achieved with the $La_{1.8}Gd_{0.2}Zr_2O_7$ layer and are respectively 91 K and 1.4 $MA.cm^{-2}$. This trend seems to be due to an improvement of the surface quality of the Ni5%W substrate by the addition of a thin seed layer. Our results offer the potential of the $La_{2-x}Gd_xZr_2O_7$ seed layers as a promising alternative for the classic Ni-5%W/LZO/CeO_2/YBCO architectures.

Introduction

The second generation of high temperature superconductor tapes, called coated conductors, presents a considerable interest for magnetic-field and electric-power applications, such as power cables, transformers and current limiters.[1] However the development of low cost and an industrial scalable manufacturing process remains crucial to develop these technologies. The combination of Chemical Solution Deposition methods (CSD) and rolling assisted biaxially textured substrates (RABiTS) is considered as one of the most promising approaches towards the fabrication of long length and low cost superconductor tapes.[2]

These coated conductors are based on $REBa_2Cu_3O_{7-x}$ (REBCO with RE = Rare Earth = Y, Gd, Nd, Sm, Eu) layers deposited on a Ni-5%W bi-axially textured substrate coated with intermediate buffer layers.[3] In this architecture, the buffer layer is an essential ingredient because it acts as a crystallographic template for the growth of the superconducting layer and chemically insulates the superconducting layer from the metallic substrate. Therefore, any candidate buffer material must obey several criteria: i) similar lattice parameters with both substrate and REBCO layer to promote epitaxial growth, ii) limit the oxidation of the metallic substrate during deposition of the superconducting film and iii) prevent the nickel diffusion from the substrate to the superconducting layer. Several materials have been considered as potential buffer layers, as $RE_2Zr_2O_7$ with RE = La or Gd,[4,5,6] YSZ,[7] Y_2O_3[8] and CeO_2.[9] $La_2Zr_2O_7$ (LZO) is currently the most promising candidate due to a relatively low formation temperature of 1000°C, a high stability up to 1500°C and a small structural lattice mismatch with the REBCO layer; close to 1% with $YBa_2Cu_3O_{7-x}$ (YBCO).[3] However the typical current density (Jc) values of Ni-5%W/LZO/CeO_2/REBCO tapes remains close to 1 $MA.cm^{-2}$ and these performances have to be improved for industrial applications.[4] The key parameter is the improvement of the texture transfer from the metallic substrate to the superconducting layer. One of the limited parameters is the quite large structural lattice mismatch between LZO and Ni-W5% (7.5%) which reduces the texture transfer between the substrate and the buffer layer.

Consequently, we have substituted in our previous works La^{3+} by Ga^{3+} to decrease the structural lattice mismatch between the buffer layer and the substrate.[10] We successfully deposited 60-nm-thick $La_{2-x}Gd_xZr_2O_7$ (LGZO) layers on a Ni-5%W substrate by the chemical solution method and we obtained a solid solution with x between 0.1 and 0.8. Unfortunately no direct improvement of the texture quality for a 60-nm-thick LGZO layer compared to a 60-nm thick LZO layer is observed. However we noticed a decrease of the roughness of the buffer layer as a function of the gadolinium percentage. This result is very interesting because a smooth surface is very important for the epitaxial growth of the YBCO layer.[3]

In our present research, we decided to deposit successively a thin LGZO layer and a thick LZO layer on a Ni-5%W substrate. LGZO will serve as seed layer or texture template for the growth of the LZO layer and will strongly decrease its roughness. However we

[a] University of Grenoble Alpes, Institut NEEL, F-38042 Grenoble, France. E-mail: herve.muguerra@hotmail.fr
[b] CNRS, Institut NEEL, F-38042 Grenoble, France
[c] .EMAT, University of Antwerp, B-2020 Antwerp, Belgium

should also keep the very good texture quality for the LZO layer. Consequently, it is important to optimize the gadolinium ratio and the thickness of the seed layer to obtain the best compromise between roughness and texture.

We decided to realize two different gadolinium contents (x = 0.2 and x = 0.8) with three different thicknesses for these compositions (20 nm, 40 nm, 60 nm). Then we deposited successively a 60-nm-thick LZO layer and a 300-nm-thick $Y_{0.5}Gd_{0.5}Ba_2Cu_3O_{7-x}$ layer (Gd-YBCO). We employed Gd-doped YBCO because the critical transition temperature (Tc) and the critical current density (Jc) of the bulk materials are reported to be higher than the ones of YBCO; Tc increased from 88 to 91 K and Ic increased from 55 to 122 $A.cm^{-2}$.[11]

This paper reports the synthesis by soft chemistry methods of a full structure consisting of a Ni-5%W/LGZO/LZO/Gd-YBCO layer stack. We determined the influence of a LGZO seed layer on the growth process of LZO and of Gd-YBCO layers as a function of the Gd content of the LGZO layer and as a function of the LGZO thickness. Finally, we investigated the superconducting properties of the different coated conductors.

Experimental

Solution preparation and film deposition

Highly biaxial textured Ni-5%W tapes provided by EVICO (Dresden) are employed as substrate for the different superconductor tapes. Prior to coating, the substrates are first cleaned in an ultrasonic bath for 15 minutes with acetone and then methanol for removing all organic traces. Then, they are heated up to 800°C for 1 hour under a continuous flow of Ar-5%H_2 gas.

For the buffer layer stacks, we employed the same two steps chemical deposition method for the different samples. First we deposited a $La_{2-x}Gd_xZr_2O_7$ layer on the substrate and secondly a $La_2Zr_2O_7$ layer on top of this layer. After each coating, the sample is heated at 450°C for 1 hour under primary vacuum and then annealed at 1000°C for 30 minutes under Ar-5%H_2 gas flow.

The precursor solutions are prepared by mixing a stoichiometric amount of lanthanum (III) 2,4-pentanedionate, gadolinium (III) 2,4-pentanedionate and zirconium (IV) 2,4-pentanedionate in propionic acid. For $La_{2-x}Gd_xZr_2O_7$ solutions, we realized three different concentrations 0.15, 0.3 and 0.6 $mol.L^{-1}$ leading to a thickness of respectively 20, 40 and 60 nm. For the $La_2Zr_2O_7$ solution, we employed a constant concentration 0.6 $mol.L^{-1}$ for a thickness close to 60 nm. The obtained solutions are all yellow/orange transparent and their viscosities are between 2.5 and 3.5 mPa.s. The precursor layers are deposited by dip-coating at a constant speed of 66 $mm.min^{-1}$ and they are dried with infrared lamps for 2 minutes at 60°C before annealing.

The $Y_{0.5}Gd_{0.5}Ba_2Cu_3O_{7-x}$ layer (Gd-YBCO) is grown on the top of the $La_2Zr_2O_7$ layer via a MOCVD reel-to-reel system in PerCoTech described in details elsewhere.[12] The thickness is close to 300 nm.

We also realized Ni-5%W/$La_2Zr_2O_7$/$Y_{0.5}Gd_{0.5}Ba_2Cu_3O_{7-x}$ tapes with the same film deposition method used for the tapes with the seed layers. This sample is a reference to compare the superconducting properties of the different coated conductors.

Characterization and analysis

The crystallographic phase and texture of the layers are investigated using a Seifert four circles diffractometer equipped with a Cu Kα source at room temperature in air. The in-plane and out-plane texture of the $La_2Zr_2O_7$ layers are determined from ϕ-scans of the LZO(222) reflection and ω-scans of the LZO(400) reflection in the rolling direction (RD) and transverse direction (TD) of the Ni-5%W tapes. For Gd-YBCO, the (103) and (005) reflections are used to characterized respectively the in-plane and out-plane texture.

Transmission electron microscopy (TEM), high angle annular dark field scanning transmission electron microscopy (HAADF STEM) and energy dispersive X-ray spectroscopy (EDX) were used in an FEI Titan "cubed" electron microscope equipped with an aberration corrector for the probe-forming lens or an FEI Osiris instrument. Both microscopes are fitted with a "Super-X" wide solid angle EDX detector. Atomic force microscopy (AFM, Veeco D3100) and EM were used to determine the thickness, the morphology, the chemical composition and the roughness of the layers.

The crystallinity and the texture at the surface of the $La_2Zr_2O_7$ layers are determined by electron backscattering diffraction (EBSD) measurements. The working distance is 11 mm with an acceleration voltage of 20 kV. The Kikuchi patterns were automatically analyzed by the data handling software package (Oxford Channel5 Software).

We determined the superconducting transition temperature (Tc) by resistivity measurements as a function of temperature and the critical current density (Jc) is determined at 77 K by the third-harmonic measurement method (CRYOSCAN, Theva).[13]

Results and discussion

The influence of a LGZO seed layer on the growth process of LZO

Figure 1 represents the X-ray θ-2θ patterns of the $La_{1-x}Gd_xZr_2O_7$ seed layers and of the $La_{1-x}Gd_xZr_2O_7$/$La_2Zr_2O_7$ buffer layer stacks as a function of the seed layer thickness, for the different gadolinium ratios x = 0.2 and 0.8.

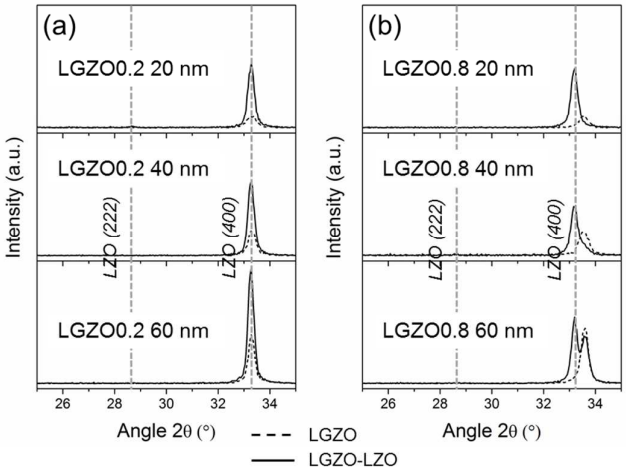

Fig. 1: X-ray θ-2θ patterns of (a) the $La_{1.8}Gd_{0.2}Zr_2O_7$/$La_2Zr_2O_7$ and (b) $La_{1.2}Gd_{0.8}Zr_2O_7$/$La_2Zr_2O_7$ buffer layer stacks as a function of the seed layer thickness.

The different oxide layers can be indexed as $La_2Zr_2O_7$ pyrochlore with a slight shift of lattice parameters as a function of gadolinium content: 10.80 Å for $La_2Zr_2O_7$ (LZO), 10.75 Å for $La_{1.8}Gd_{0.2}Zr_2O_7$ (LGZO0.2) and 10.65 Å for $La_{1.2}Gd_{0.8}Zr_2O_7$ (LGZO0.8). For all the patterns, we only observe the (400) peaks and the undesired (222) peak is not detected showing a very strong c-axis preferred orientation of the buffer layers on the Ni-5%W substrate. For the LGZO0.2/LZO series, only one (400) peak is detected and the intensity increases as a function of the seed layer thickness. This feature is consistent with an adjustment of the lattice parameters close to 10.78 Å for the two layers. The behavior of the LGZO0.8/LZO series is quite different, the intensity of the (400) peak is almost constant and we observe a splitting of the (400) peak for the 60-nm-thick LGZO0.8 layer. This trend is due to the relatively large difference of lattice parameter between LGZO0.8 and LZO, respectively 10.65 Å and 10.80 Å.

We determined for the different samples the in-plane and out-plane texture of the top $La_2Zr_2O_7$ layer by respectively ϕ-scans of the LZO(222) reflection and ω-scans of the LZO(400) reflection in the rolling direction (RD) and transverse direction (TD) of the Ni-5%W tapes (Figure 2).

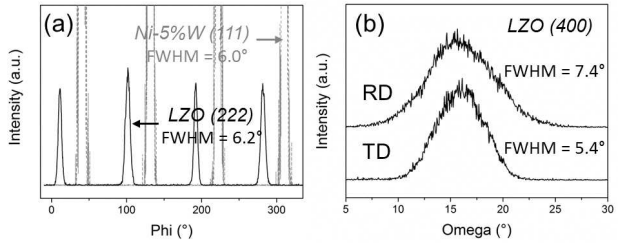

Fig. 2: (a) ϕ-scan of the LZO(222)and Ni-5%W(111) reflections and (b) ω-scans of the LZO(400) reflection in the rolling direction (RD) and transverse direction (TD) of the Ni-5%W tapes for the 20-nm-thick LGZO0.2/LZO sample.

We observe a similar behavior for the average full widths at half maximum (FWHM) values of the LGZO0.2/LZO and LGZO0.8/LZO series (Figure 3). The quality of the in-plane texture and of the out-plane texture in the TD is similar to the values measured for a single layer of 60-nm-thick $La_2Zr_2O_7$. The FWHM values are respectively close to 6° and 5.2°.

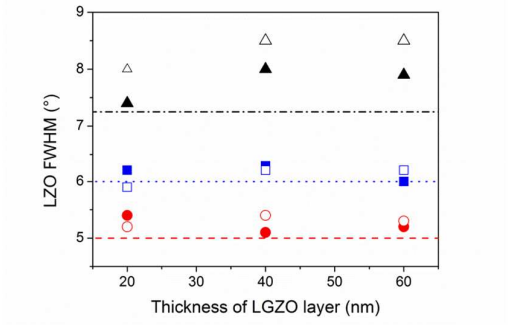

Fig. 3: Variation of the FWHM values across the LGZO0.2/LZO (closed symbols) and LGZO0.8/LZO (open symbols) series as a function of the seed layer thickness. (■) = ϕ-scan, (▲) = ω-scans RD, (●) = ω-scans TD.

For the out-plane texture in the RD we observe a decrease of the texture quality as a function of the seed layer thickness. Indeed the FWHM values are larger than the ones measured for a single layer of $La_2Zr_2O_7$, respectively 7.2° for LZO and between 7.4° and 8.5° with the seed layer. Nevertheless these values are still in the appropriate range for the deposition of REBCO layers with a high critical current density.[14]

The thickness of the LGZO/LZO buffer layer stacks is confirmed by TEM cross-section analysis. The thickness of LZO layer remains close to 60 nm and the thickness of different LGZO layers are 20 nm, 40 nm and 60 nm for LGZO0.2 and LGZO0.8 (Figure 4a).

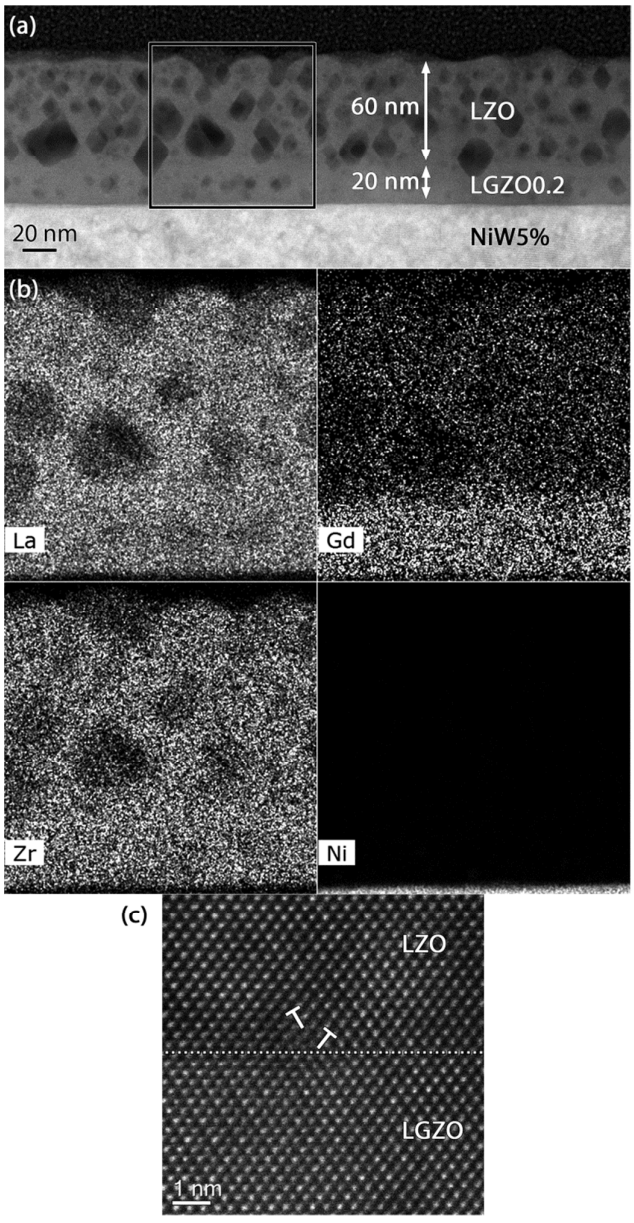

Fig. 4: (a) HAADF STEM image of the 20-nm-thick LGZO0.2/LZO buffer layer on a Ni-5%W substrate in cross section. (b) EDX maps of La, Gd, Zr and Ni. The residual intensity in the LZO area in the Gd map is caused by the background noise signal and by a relatively small Gd concentration in the LGZO (c) High resolution cross section

HAADF STEM image of the LGZO0.8/LZO buffer layer interface (dashed line) with two (110) edge dislocations.

For the different samples, TEM also clearly identifies the two separate layers of the stack and EDX mapping confirms that there is no diffusion of nickel throughout the buffer layer and that the gadolinium is mostly located in the seed layer (Figure 4b). For the LGZO0.8-LZO buffer layer, the relatively important difference of cell parameters between LZO and LGZO0.8 layers is leading to the formation of (110) edge dislocations at the interphase boundary (Figure 4c). For all the samples, the LZO and LGZO layers contain pores also called nanovoids. However in the 20-nm-thick seed layer we observe a dramatic decrease of the pore density and of the pore size (Figure 4a). This result confirms the observations by Cloet et al. for a stack composed of a 20-nm-thick $La_2Zr_2O_7$ seed layer and of a 100-nm-thick $La_2Zr_2O_7$ on a Ni-W5% substrate.[15] Indeed the thickness of the seed layer is close to the diameter of one LGZO grain (20 nm) and consequently the formation of the pores throughout the layer is reduced. A denser seed layer is a very interesting result and will be an advantage to improve the protection of the substrate from oxidation during the Gd-YBCO growth.

AFM investigations of the surface morphology of the top LZO layers show an homogenous and crack free surface for the different samples (Figure 5). The shape of the grains is regular with a narrow particle size distribution. The gadolinium percentage of the seed layer seems to have no direct impact on the evolution of the grain diameter of the LZO layer. However the particle size is different as a function of the seed layer thickness, close to 20 nm for 20-nm-thick, 30 nm for the 40-nm-thick and 25 nm for a 60-nm-thick LGZO layer (Figure 5).

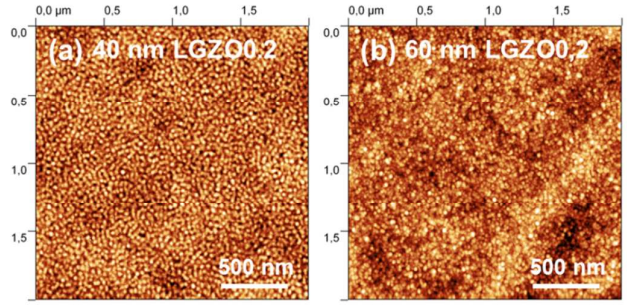

Fig. 5: AFM images of LGZO0.2/LZO buffer layers as a function of the seed layer thickness.

We measured the root mean square roughness (RMS) of the LZO layers on 4 μm^2 square samples (Figure 6).

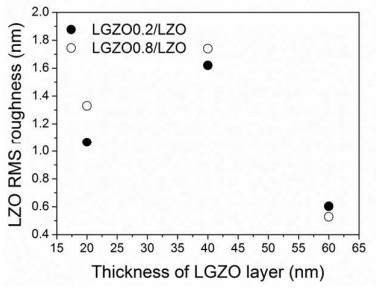

Fig. 6: Variation of the RMS roughness for LGZO0.2/LZO and LGZO0.8/LZO buffer layers as a function of the seed layer thickness.

The RMS values are between 0.5 nm and 1.8 nm and they follow the same trend as the grain size. The RMS values reported by Knoth and al. for a single 100-nm-thick LZO layer and a double LZO layer on Ni-W5% substrate are respectively 1.9 nm and 2.3 nm.[16] Consequently, we can conclude that the LGZO seed layer greatly decreases the roughness of the LZO layer. This result is very promising for epitaxial growth of a Gd-YBCO layer on the top of the LZO layer.

We characterized the crystallinity and texture quality at the surface of the LZO layers by the EBSD technique. For the different LGZO/LZO layers, we realized a 360 µm × 480 µm map as a function of the orientation deviation from the ideal LZO <011> (100) direction (Figure 7).

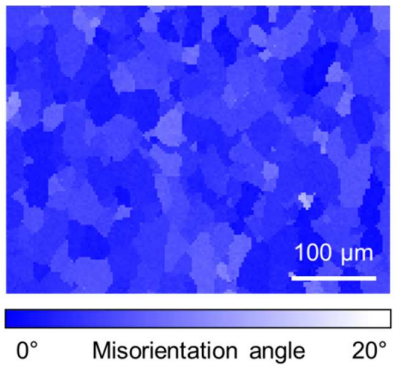

Fig. 7: Misorientation map of a 20-nm-thick LGZO0.2/LZO buffer layer.

An indexing rate between 90% and 95% is obtained for the different samples because of the highly crystalline surfaces. We extracted from this map the distribution of the angle deviation for the ideal LZO <011> (100) direction (Figure 8).

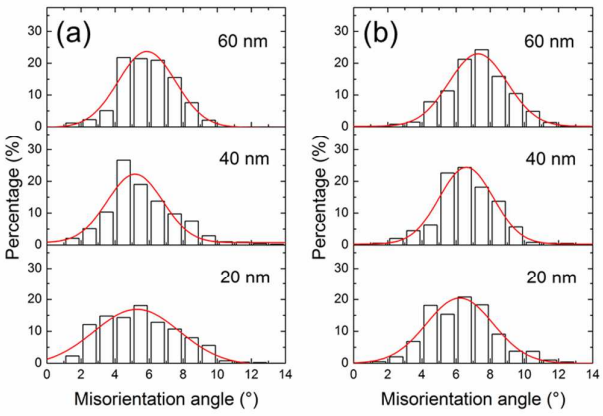

Fig. 8: Distribution of the angle deviation from the ideal LZO <011> (100) direction for (a) LGZO0.2/LZO and (b) LGZO0.8/LZO buffer layers as a function of the seed layer thickness.

For the different samples, the distribution can be described by a Gaussian function. We observe a shift of the maximum percentage value as a function of the seed layer thickness, from 5° to 6° for LGZO0.2 and from 6° to 7.5° for LGZO0.8 (Figure 8). However the indexing part with a misorientation below 10° remains close to 90% for the different samples. As a conclusion, the misorientation at the

surface of the LZO layer is mainly below the limit value to achieve high Jc values and we can expect a good connection between the Gd-YBCO grains[14].

Structural and superconducting properties of the Gd-YBCO layers

Summarizing our different results on the LGZO/LZO series, we can conclude that the most promising candidates for superconductor tapes are the buffer layer stacks with a thin seed layer for the two different gadolinium ratios x = 0.2 and x = 0.8. Indeed these configurations are the best compromise to achieve a good texture and a low roughness. Consequently, we have decided to deposit a 300-nm-thick Gd-YBCO layer by MOCVD only on the buffer layers with a 20-nm-thick seed layer.

We realized X-ray diffraction θ-2θ scans of the different samples (see an example on Figure 9). We observe no $NiWO_4$ and no NiO peaks and only peaks of the Gd-YBCO layer, of the buffer layers and of the Ni-W5% substrate. As a conclusion, a 80-nm-thick LGZO/LZO buffer layer seems to be a relative efficient barrier to oxygen and allows a good texture transfer from the substrate throughout the Gd-YBCO layer.

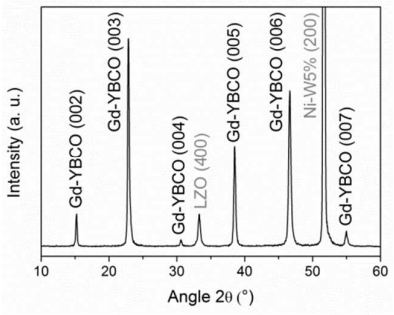

Fig. 9: X-ray diffraction patterns of Ni-5%W/LGZO0.2/LZO/Gd-YBCO tapes.

We also determined the in-plane and out-plane texture of the Gd-YBCO layer by respectively ϕ-scans of the Gd-YBCO(103) reflection and ω-scans of the Gd-YBCO(005) reflection in the rolling direction (RD) and transverse direction (TD) of the Ni-5%W tapes. The FWHM values measured for Ni-5%W, LZO and Gd-YBCO layers are summarized in table 1.

Table 1: In-plane and out-of-plane texture of Ni-5%W substrate, LGZO/LZO and Gd-YBCO layers. Reflections of Ni-5%W(111), LZO(222), Gd-YBCO(103) are used in the ϕ-scans, while Ni-5%W(200), LZO(400), Gd-YBCO(005) are used in the ω scan.

Layers	FWHM ϕ-scan (°)	FWHM ω scan TD (°)	FWHM ω scan RD (°)
Ni-5%W substrate	6.0	4.7	7.4
LGZO0.2/LZO	6.2	5.4	7.4
LGZO0.2/LZO/Gd-YBCO	6.6	4.2	6.4
LGZO0.8/LZO	5.9	5.2	8.0
LGZO0.8/LZO/Gd-YBCO	6.8	4.5	6.9

For the different samples, we observe a very good texture transfer from the substrate to the Gd-YBCO layer. Indeed the FWHM values of the ω-scans remain close to 4.5° in TD and decrease from 7.4° to 6.4° in RD. Nevertheless the FWHM values of the ϕ-scans slightly increase from 6° to 6.8°, but these values are still below the ones reported by Zhao et al..[5] Indeed Zhao et al. observe a gradual degradation of the texture quality from the substrate to the YBCO layer due to different factors such as roughness of the successive layers or development of defects during the growth process.

Figure 10a shows a HAADF-STEM image of the coated conductor samples with a Ni-5%W/LGZO/LZO/YBCO architecture viewed in cross-section.

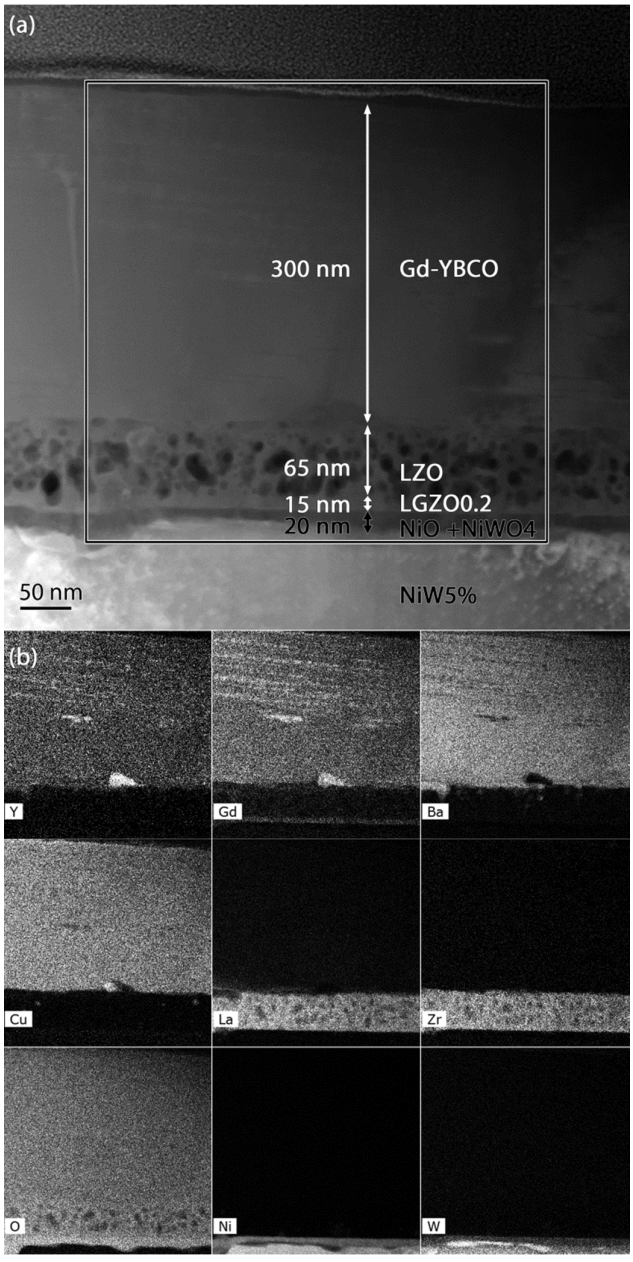

Fig. 10: (a) HAADF STEM image of a Ni-5%W/LGZO0.2/LZO/Gd-YBCO tape in cross section. (b) EDX maps of Y, Gd, Ba, Cu, La, Zr and Ni. Residual intensity in the LZO area in the Gd map is caused by background noise signal and by a relatively small Gd concentration in LGZO.

The thickness of the Gd-YBCO layer is close to 300 nm and close to 80 nm for the buffer layer. A 10 nm thin dark contrast band above the Ni-5%w substrate is observed. The EDX measurements show that this layer corresponds to the NiO layer with $NiWO_4$ phase inclusions on the Ni-NiO interface. Such dramatic change of contrast in the HAADF image is directly related to a change indensity and average Z value between Ni/W and $NiO/NiWO_4$. The contrast dependence on oxygen concentration has been established on different materials by of Kim et al[17] and Lin et al[18] This result proves that we have a small oxidation of the metallic substrate after the deposition of the superconducting film. However it is very difficult with the chemical deposition methods to completely prevent this feature; similar results are also observed by other groups.[9] We also carried out an EDX mapping of the entire superconducting tapes and no diffusion of nickel in the buffer layers or in the superconducting layer is noticed (Figure 10b).

The Y- and Gd-rich planar structures, shown in Figure 10b, are actually epitaxially grown $Y_{2-x}Gd_xO_3$ particle agglomerates in the Gd-YBCO matrix (Figure 11); Gd-YBCO [001] // $Y_{2-x}Gd_xO_3$ [001] and Gd-YBCO [100] // $Y_{2-x}Gd_xO_3$ [1-10]. The thickness of the $Y_{2-x}Gd_xO_3$ lamellas along the $[001]_{Gd\text{-}YBCO}$ direction is below 10 nm. Also these inclusions induce distortions in the structure of the superconducting layer in the form of e.g. stacking faults. This result is very interesting because nanoparticles such as $BaZrO_3$,[19] Y_2O_3[20] or Gd_2O_3[21] may act as pinning centers in REBCO films. Moreover high vortex pinning forces lead to high critical currents.

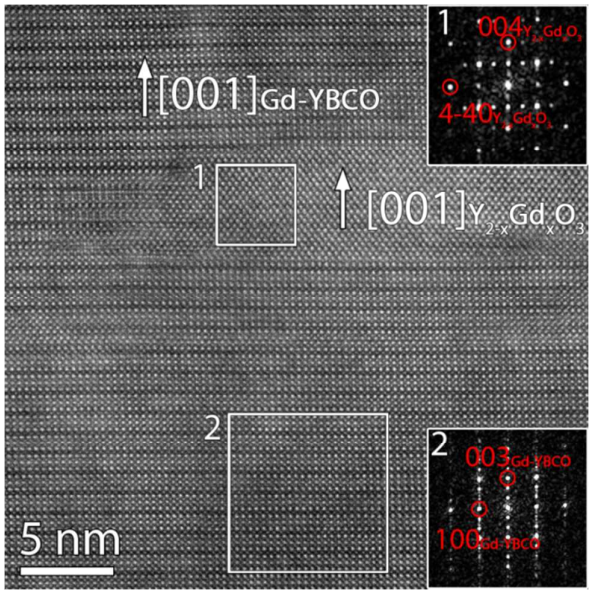

Fig. 11: HAADF STEM Z-contrast image showing the presence of a $Y_{2-x}Gd_xO_3$ particle in the Gd-YBCO matrix. Two FFT insets from the corresponding areas in the main image show that Gd-YBCO [001] // $Y_{2-x}Gd_xO_3$ [001] and Gd-YBCO [100] // $Y_{2-x}Gd_xO_3$ [1-10].

Finally, we studied the superconducting properties of the different coated conductors. First, we measure the variation of the resistivity with no magnetic field as a function of temperature for the different tapes (Figure 12). For the different samples, the Tc is between 88.5 and 91 K with a sharp transition close to ΔTc = 1 indicating a good oxygenation of the superconducting layer and an homogenous interconnectivity between the Gd-YBCO grains.[22]

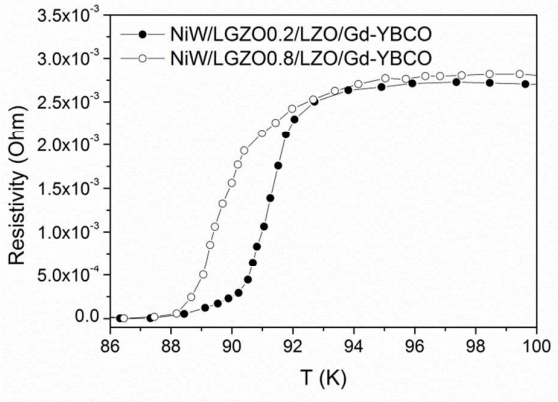

Fig. 12: Variation of the resistivity with no magnetic field as a function of temperature for the different tapes.

We determined the Jc values at 77 K of the different tapes (Figure 13). The Jc values of the tapes with a LGZO seed layer are both higher than the reference Ni-5%W/LZO/Gd-YBCO; respectively 0.9 $MA.cm^{-2}$ with only LZO, 1.1 $MA.cm^{-2}$ with LGZO0.8-LZO and 1.4 $MA.cm^{-2}$ with LGZO0.2-LZO. As a conclusion, the original Ni-5%W/LGZO0.2/LZO/Gd-YBCO tape is the most promising architecture for the fabrication of high Jc and low cost superconductor tapes. Indeed the Jc value measured for this sample is also higher than the one reached by REBCO tapes using $La_2Zr_2O_7/CeO_2$ and $Gd_2Zr_2O_7/Ce_{0.9}La_{0.1}O_2$ buffer layers deposited by chemical solution methods on a Ni-5%W substrate.[4,5]

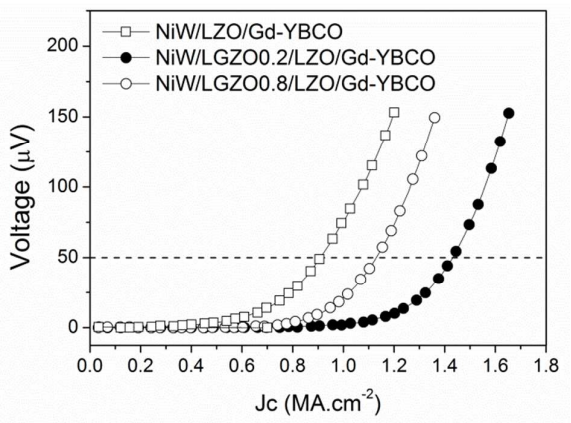

Fig. 13: Determination the Jc values at 77 K of the different tapes.

This result can be explained by an improvement of the surface quality of the Ni5%W substrate. Indeed the insertion of a thin LGZO layer with a low roughness and a high texture quality before the LZO layer seems to be a promising method to improve the texture transfer from the substrate to the superconducting layer.

Conclusions

By chemical methods we have deposited a $La_{2-x}Gd_xZr_2O_7$ seed layer on a Ni-5%W substrate to improve the performance of the classic Ni-5%W/$La_2Zr_2O_7$/$REBa_2Cu_3O_{7-x}$ tapes. For two different gadolinium ratios x = 0.2 and 0.8, we investigated the influence of the seed layer thickness on the texture quality and on the roughness of the $La_2Zr_2O_7$ layers. The most promising

buffer layer stacks are realized with a 20-nm-thick $La_{1.8}Gd_{0.2}Zr_2O_7$ layer and a 20-nm-thick $La_{1.2}Gd_{0.8}Zr_2O_7$. Indeed these $La_{2-x}Gd_xZr_2O_7/La_2Zr_2O_7$ buffer layers present a good texture quality with a roughness four times lower than that of a $La_2Zr_2O_7$ layer. Moreover the top layers show a low misorientation at the surface compared to the ideal $La_2Zr_2O_7$ <011> (100) direction. We deposited a 300-nm layer of $Y_{0.5}Gd_{0.5}Ba_2Cu_3O_{7-x}$ by MOCVD on the best buffer layer stacks. We observe a good texture transfer from the substrate throughout the superconducting layer and we measured higher Jc values for Ni-5%W/$La_{2-x}Gd_xZr_2O_7/La_2Zr_2O_7/Y_{0.5}Gd_{0.5}Ba_2Cu_3O_{7-x}$ tapes than for the classic Ni-5%W/$La_2Zr_2O_7/CeO_2/YBa_2Cu_3O_{7-x}$ tapes. The best Jc values at 77 K are obtained with a 20-nm-thick $La_{1.8}Gd_{0.2}Zr_2O_7$ seed layer and are close to 1.4 $MA.cm^{-2}$. The relatively high performance of these new tapes seem due to an improvement of the surface quality of the Ni5%W substrate by the addition of a thin LGZO seed layer. In conclusion, the $La_{2-x}Gd_xZr_2O_7/La_2Zr_2O_7$ buffer layer stacks are very promising as an alternative for $La_2Zr_2O_7/CeO_2$ to realize high Jc coated conductors.

Acknowledgements

This work was performed within the framework of the EUROTAPES project (FP7-NMP.2011.2.2-1 Grant no. 280438), funded by the European Union. The authors also thank L. Porcar and P. Chometon for superconducting transition temperature and critical current density measurements and P. Odier for fruitful discussion.

Notes and references

1. S. Nishijima, S. Eckroad, A. Marian, K. Choi, W.S. Kim, M. Terai, Z. Deng, J. Zheng, J. Wang, K. Umemoto, J. Du, P. Febvre, S. Keenan, O. Mukhanov, L.D. Cooley, C.P Foley, W.V. Hassenzahl and M. Izumi, *Supercond. Sci. Technol.,* 2013, **26**, 113001.
2. X. Obradors et al, *Supercond. Sci. Technol.,* 2004, **17**, 1055–64.
3. V. Narayanan and I. Van Driessche, *Progress in Solid State Chemistry*, 2012, **40**, 57.
4. T. Caroff, S. Morlens, A. Abrutis, M. Decroux, P. Chaudouët, L. Porcar, Z. Saltyte, C. Jiménez, P. Odier and F. Weiss, *Supercond. Sci. Technol.,* 2008, **21**, 075007.
5. Y. Zhao, X.F. Li, A. Khoryushin, D. He, N.H. Andersen, J.B. Hansen and J.C. Grivel, *Supercond. Sci. Technol.,* 2012, **25**, 015008.
6. Y. Zhao, L. Ma, W. Wu, H.-L. Suob and J.-C. Grivel, *J. Mater. Chem. A*, 2015, **3**, 13275.
7. D.M. Feldmann, T.G. Holesinger, B. Maiorov, H. Zhou, S.R. Foltyn, J.Y. Coulter and I. Apodoca, *Supercond. Sci. Technol.*, 2010, **23**, 115016.
8. M.S. Bhuiyan, M. Paranthaman, S. Kang, D.F. Lee and K. Salama, *Physica C*, 2005, **422**, 95-101.
9. V. Narayanan, P. Lommens, K. De Buysser, D.E.P. Vanpoucke, R. Huehne, L. Molina, G. Van Tendeloo, P. Van Der Voorta and I. Van Driessche, *J. Mater. Chem.,* 2012, **22**, 8476.
10. H. Muguerra, A.C. Pescheux and J.L. Soubeyroux, *Journal of Physics: Conference Series, 2014,* **507**, 022022.
11. K. Öztürk, S. Celik, U. Cevik and E. Yanmaz, *Journal of Alloys and Compounds,* 2007, **433**, 46–52O. Stadel and R. Muydinov, *IEEE/CSC & ESAS European Superconductivity News Forum, 2009,* **No. 9**.
12. O. Stadel and R. Muydinov, *IEEE/CSC & ESAS European Superconductivity News Forum, 2009,* **No. 9**.
13. Y. Mawatari, H. Yamasaki and Y. Nakagawa, *Appl. Supercond.,* 2003, **13**, 3710.
14. D. Dimos, P. Chaudhari and J. Mannhart, *Phys. Rev.*, 1990, **41**, 4038.
15. V. Cloet, P. Lommens, R. Hühne, K. De Buysser, S. Hoste and I. Van Driessche, *Journal of Crystal Growth,* 2011, **325**, 68–75.
16. K. Knoth, R. Hühne, S. Oswald, L. Molina, O. Eibl, L. Schultz and B. Holzapfel, *Thin Solid Films,* 2008, **516**, 2099–2108.
17. Kim, Y. M. et al, *Nat. Mater., 2012*, **11**, 888–894
18. Lin Yet al, *Nat Commun*, 2015, **6**
19. J.L. MacManus-Driscoll et al, *Nat. Mater.,* 2004, **3**, 439.
20. H. Wang, A. Serquis, B. Maiotov, L. Civale, Q.X. Jia, P.N. Arent, S.R. Foltyn, J.L. MacManus-Driscoll and X. Zhang, *J. Appl. Phys.,* 2006, **100**, 053904.
21. S. Xu, X.S. Wu, G.B. Ma, Z.H. Wang and J. Gao, *J. of Appl. Phys.,* 2008, **103**, 07C714.
22. D.X. Chen, R.B. Goldfarb, J. Nogues and K.V. Rao, *J. Appl. Phys.,* 1988, **63**, 980.

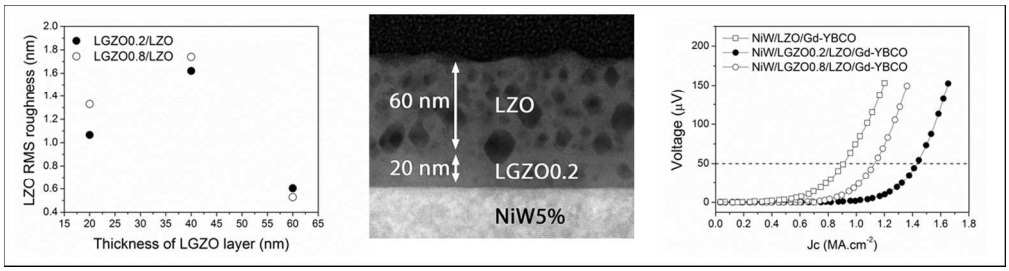

233x60mm (150 x 150 DPI)